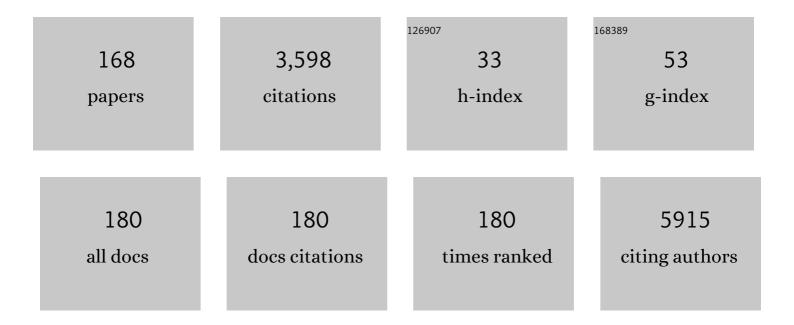
## David Moratal

List of Publications by Year in descending order

Source: https://exaly.com/author-pdf/3748294/publications.pdf Version: 2024-02-01



#	Article	IF	CITATIONS
1	Erbb4 Deletion from Fast-Spiking Interneurons Causes Schizophrenia-like Phenotypes. Neuron, 2013, 79, 1152-1168.	8.1	254
2	Role of material-driven fibronectin fibrillogenesis in cell differentiation. Biomaterials, 2011, 32, 2099-2105.	11.4	122
3	Effect of nanoscale topography on fibronectin adsorption, focal adhesion size and matrix organisation. Colloids and Surfaces B: Biointerfaces, 2010, 77, 181-190.	5.0	108
4	Classifying brain metastases by their primary site of origin using a radiomics approach based on texture analysis: a feasibility study. European Radiology, 2018, 28, 4514-4523.	4.5	106
5	Left orbitofrontal and superior temporal gyrus structural changes associated to suicidal behavior in patients with schizophrenia. Progress in Neuro-Psychopharmacology and Biological Psychiatry, 2008, 32, 1673-1676.	4.8	105
6	Schizophrenia with auditory hallucinations: A voxel-based morphometry study. Progress in Neuro-Psychopharmacology and Biological Psychiatry, 2008, 32, 72-80.	4.8	100
7	Opportunistic screening for osteoporosis by routine CT in Southern Europe. Osteoporosis International, 2017, 28, 983-990.	3.1	94
8	Substrate-Induced Assembly of Fibronectin into Networks: Influence of Surface Chemistry and Effect on Osteoblast Adhesion. Tissue Engineering - Part A, 2009, 15, 3271-3281.	3.1	91
9	Metabolomic Profile of Human Myocardial Ischemia by Nuclear Magnetic Resonance Spectroscopy of Peripheral Blood Serum. Journal of the American College of Cardiology, 2012, 59, 1629-1641.	2.8	84
10	Fibronectin adsorption and cell response on electroactive poly(vinylidene fluoride) films. Biomedical Materials (Bristol), 2012, 7, 035004.	3.3	83
11	Support vector machine classification of brain metastasis and radiation necrosis based on texture analysis in MRI. Journal of Magnetic Resonance Imaging, 2015, 42, 1362-1368.	3.4	83
12	Differentiation between acute and chronic myocardial infarction by means of texture analysis of late gadolinium enhancement and cine cardiac magnetic resonance imaging. European Journal of Radiology, 2017, 92, 78-83.	2.6	79
13	Role of Surface Chemistry in Protein Remodeling at the Cell-Material Interface. PLoS ONE, 2011, 6, e19610.	2.5	78
14	Texture analysis of cardiac cine magnetic resonance imaging to detect nonviable segments in patients with chronic myocardial infarction. Medical Physics, 2018, 45, 1471-1480.	3.0	64
15	Emotional words induce enhanced brain activity in schizophrenic patients with auditory hallucinations. Psychiatry Research - Neuroimaging, 2007, 154, 21-29.	1.8	60
16	Role of superhydrophobicity in the biological activity of fibronectin at the cell–material interface. Soft Matter, 2011, 7, 10803.	2.7	58
17	Estimation of atrial fibrillatory wave from single-lead atrial fibrillation electrocardiograms using principal component analysis concepts. Medical and Biological Engineering and Computing, 2005, 43, 557-560.	2.8	57
18	Chronic Auditory Hallucinations in Schizophrenic Patients: MR Analysis of the Coincidence between Functional and Morphologic Abnormalities. Radiology, 2007, 244, 549-556.	7.3	57

#	Article	IF	CITATIONS
19	Incubation of neural alcohol cue reactivity after withdrawal and its blockade by naltrexone. Addiction Biology, 2020, 25, e12717.	2.6	57
20	Prognostic and therapeutic implications of dipyridamole stress cardiovascular magnetic resonance on the basis of the ischaemic cascade. Heart, 2008, 95, 49-55.	2.9	54
21	Automatic segmentation and 3D reconstruction of intravascular ultrasound images for a fast preliminar evaluation of vessel pathologies. Computerized Medical Imaging and Graphics, 2007, 31, 71-80.	5.8	53
22	Prediction of Reverse Remodeling at Cardiac MR Imaging Soon after First ST-Segment–Elevation Myocardial Infarction: Results of a Large Prospective Registry. Radiology, 2016, 278, 54-63.	7.3	49
23	Different theta frameworks coexist in the rat hippocampus and are coordinated during memory-guided and novelty tasks. ELife, 2020, 9, .	6.0	47
24	Prognostic Implications of Dipyridamole Cardiac MR Imaging: A Prospective Multicenter Registry. Radiology, 2012, 262, 91-100.	7.3	46
25	Texture Analysis in Magnetic Resonance Imaging: Review and Considerations for Future Applications. , 0, , .		43
26	k-Space tutorial: an MRI educational tool for a better understanding of k-space. Biomedical Imaging and Intervention Journal, 2008, 4, e15.	0.5	42
27	Identification of the presence of ischaemic stroke lesions by means of texture analysis on brain magnetic resonance images. Computerized Medical Imaging and Graphics, 2019, 74, 12-24.	5.8	42
28	Differentiation of mesenchymal stem cells in chitosan scaffolds with double micro and macroporosity. Journal of Biomedical Materials Research - Part A, 2010, 95A, 1182-1193.	4.0	41
29	Subtle variations in polymer chemistry modulate substrate stiffness and fibronectin activity. Soft Matter, 2010, 6, 4748.	2.7	41
30	Surface mobility regulates skeletal stem cell differentiation. Integrative Biology (United Kingdom), 2012, 4, 531.	1.3	39
31	Vasodilator Stress CMR and All-Cause Mortality in Stable Ischemic Heart Disease. JACC: Cardiovascular Imaging, 2020, 13, 1674-1686.	5.3	39
32	Assessment of 2D and 3D fractal dimension measurements of trabecular bone from highâ€spatial resolution magnetic resonance images at 3 T. Medical Physics, 2010, 37, 4930-4937.	3.0	37
33	Structural and functional, empirical and modeled connectivity in the cerebral cortex of the rat. Neurolmage, 2017, 159, 170-184.	4.2	36
34	Microvascular perfusion 1 week and 6 months after myocardial infarction by first-pass perfusion cardiovascular magnetic resonance imaging. Heart, 2006, 92, 1801-1807.	2.9	35
35	Chronic alcohol consumption alters extracellular space geometry and transmitter diffusion in the brain. Science Advances, 2020, 6, eaba0154.	10.3	34
36	Convolutive Blind Source Separation Algorithms Applied to the Electrocardiogram of Atrial Fibrillation: Study of Performance. IEEE Transactions on Biomedical Engineering, 2007, 54, 1530-1533.	4.2	33

#	Article	IF	CITATIONS
37	In Vivo Trabecular Bone Morphologic and Mechanical Relationship Using High-Resolution 3-T MRI. American Journal of Roentgenology, 2008, 191, 721-726.	2.2	33
38	Microcomputed tomography and microfinite element modeling for evaluating polymer scaffolds architecture and their mechanical properties. Journal of Biomedical Materials Research - Part B Applied Biomaterials, 2009, 91B, 191-202.	3.4	33
39	Effect of ischemic postconditioning on microvascular obstruction in reperfused myocardial infarction. Results of a randomized study in patients and of an experimental model in swine. International Journal of Cardiology, 2014, 175, 138-146.	1.7	33
40	Semiautomatic computer-aided classification of degenerative lumbar spine disease in magnetic resonance imaging. Computers in Biology and Medicine, 2015, 62, 196-205.	7.0	33
41	Incidence, Outcomes, and Predictors of Ventricular Thrombus after Reperfused ST-Segment–Elevation Myocardial Infarction by Using Sequential Cardiac MR Imaging. Radiology, 2017, 284, 372-380.	7.3	32
42	Glioblastomas and brain metastases differentiation following an MRI texture analysis-based radiomics approach. Physica Medica, 2020, 76, 44-54.	0.7	32
43	MR pharmacokinetic modeling of the patellar cartilage differentiates normal from pathological conditions. Journal of Magnetic Resonance Imaging, 2008, 27, 171-177.	3.4	31
44	Controlled wettability, same chemistry: biological activity of plasma-polymerized coatings. Soft Matter, 2012, 8, 5575.	2.7	30
45	Effect of topological cues on material-driven fibronectin fibrillogenesis and cell differentiation. Journal of Materials Science: Materials in Medicine, 2012, 23, 195-204.	3.6	30
46	Brain metastases detection on MR by means of threeâ€dimensional tumorâ€appearance template matching. Journal of Magnetic Resonance Imaging, 2016, 44, 642-652.	3.4	30
47	A radiomics evaluation of 2D and 3D MRI texture features to classify brain metastases from lung cancer and melanoma. , 2017, 2017, 493-496.		30
48	Semiautomatic Analysis of Phase Contrast Magnetic Resonance Imaging of Cerebrospinal Fluid Flow through the Aqueduct of Sylvius. Magnetic Resonance Materials in Physics, Biology, and Medicine, 2006, 19, 78-87.	2.0	28
49	Schwann-cell cylinders grown inside hyaluronic-acid tubular scaffolds with gradient porosity. Acta Biomaterialia, 2016, 30, 199-211.	8.3	28
50	Resultados de la estrategia farmacoinvasiva y de la angioplastia primaria en la reperfusión del infarto con elevación del segmento ST. Estudio con resonancia magnética cardiaca en la primera semana y en el sexto mes. Revista Espanola De Cardiologia, 2011, 64, 111-120.	1.2	27
51	Fibronectin Distribution on Demixed Nanoscale Topographies. International Journal of Artificial Organs, 2011, 34, 54-63.	1.4	25
52	Non-monotonic cell differentiation pattern on extreme wettability gradients. Biomaterials Science, 2013, 1, 202-212.	5.4	25
53	2D and 3D texture analysis to differentiate brain metastases on MR images: proceed with caution. Magnetic Resonance Materials in Physics, Biology, and Medicine, 2018, 31, 285-294.	2.0	22
54	Fibrinogen Patterns and Activity on Substrates with Tailored Hydroxy Density. Macromolecular Bioscience, 2009, 9, 766-775.	4.1	21

#	Article	IF	CITATIONS
55	Role of Material-Driven Fibronectin Fibrillogenesis in Protein Remodeling. BioResearch Open Access, 2013, 2, 364-373.	2.6	21
56	Mapping Functional Connectivity in the Rodent Brain Using Electric-Stimulation fMRI. Methods in Molecular Biology, 2018, 1718, 117-134.	0.9	21
57	Vitronectin alters fibronectin organization at the cell–material interface. Colloids and Surfaces B: Biointerfaces, 2013, 111, 618-625.	5.0	20
58	Characterization of normal regional myocardial function by MRI cardiac tagging. Journal of Magnetic Resonance Imaging, 2015, 41, 83-92.	3.4	20
59	Multi-modal MRI classifiers identify excessive alcohol consumption and treatment effects in the brain. Addiction Biology, 2017, 22, 1459-1472.	2.6	17
60	Evaluating Functional Connectivity Alterations in Autism Spectrum Disorder Using Network-Based Statistics. Diagnostics, 2018, 8, 51.	2.6	17
61	Structural connectivity centrality changes mark the path toward Alzheimer's disease. Alzheimer's and Dementia: Diagnosis, Assessment and Disease Monitoring, 2019, 11, 98-107.	2.4	17
62	A Fractal Nature for Polymerized Laminin. PLoS ONE, 2014, 9, e109388.	2.5	16
63	Brain Metastases Detection Algorithms in Magnetic Resonance Imaging. IEEE Latin America Transactions, 2016, 14, 1109-1114.	1.6	16
64	Link-Level Functional Connectivity Neuroalterations in Autism Spectrum Disorder: A Developmental Resting-State fMRI Study. Diagnostics, 2019, 9, 32.	2.6	16
65	Radiomicrobiomics: Advancing Along the Gut-brain Axis Through Big Data Analysis. Neuroscience, 2019, 403, 145-149.	2.3	15
66	Analysis of the extension of Q-waves after infarction with body surface map: Relationship with infarct size. International Journal of Cardiology, 2006, 111, 399-404.	1.7	14
67	Fibronectin-matrix sandwich-like microenvironments to manipulate cell fate. Biomaterials Science, 2014, 2, 381-389.	5.4	14
68	Increased network centrality of the anterior insula in early abstinence from alcohol. Addiction Biology, 2022, 27, e13096.	2.6	14
69	Poly( <scp>L</scp> ″actide) Substrates with Tailored Surface Chemistry by Plasma Copolymerisation of Acrylic Monomers. Plasma Processes and Polymers, 2009, 6, 190-198.	3.0	13
70	Design and Assembly Procedures for Large-Sized Biohybrid Scaffolds as Patches for Myocardial Infarct. Tissue Engineering - Part C: Methods, 2014, 20, 817-827.	2.1	13
71	Functional Living Biointerphases. Advanced Healthcare Materials, 2013, 2, 1213-1218.	7.6	12
72	Neurosurgery planning in rodents using a magnetic resonance imaging assisted framework to target experimentally defined networks. Computer Methods and Programs in Biomedicine, 2015, 121, 66-76.	4.7	12

#	Article	IF	CITATIONS
73	Ejection Fraction by Echocardiography for a Selective Use of Magnetic Resonance After Infarction. Circulation: Cardiovascular Imaging, 2020, 13, e011491.	2.6	12
74	A fully automated level-set based segmentation method of thoracic and lumbar vertebral bodies in Computed Tomography images. , 2015, 2015, 3049-52.		11
75	Quantitative Analysis of Real-Time Infrared Thermography for the Assessment of Lumbar Sympathetic Blocks: A Preliminary Study. Sensors, 2021, 21, 3573.	3.8	10
76	"PINOT― Timeâ€resolved parallel magnetic resonance imaging with a reduced dynamic field of view. Magnetic Resonance in Medicine, 2011, 65, 1062-1074.	3.0	9
77	Unsupervised segmentation of brain regions with similar microstructural properties: Application to alcoholism. , 2013, 2013, 1053-6.		9
78	Computer-aided detection of brain metastases using a three-dimensional template-based matching algorithm. , 2014, 2014, 2384-7.		9
79	Micro-computed tomography image-based evaluation of 3D anisotropy degree of polymer scaffolds. Computer Methods in Biomechanics and Biomedical Engineering, 2015, 18, 446-455.	1.6	9
80	Magnetic Resonance Assessment of Left Ventricular Ejection Fraction at Any Time <scp>Postâ€Infarction</scp> for Prediction of Subsequent Events in a Large Multicenter <scp>STEMI</scp> Registry. Journal of Magnetic Resonance Imaging, 2022, 56, 476-487.	3.4	9
81	One-Week and 6-Month Cardiovascular Magnetic Resonance Outcome of the Pharmacoinvasive Strategy and Primary Angioplasty for the Reperfusion of ST-Segment Elevation Myocardial Infarction. Revista Espanola De Cardiologia (English Ed ), 2011, 64, 111-120.	0.6	8
82	Primary ciliary dyskinesia assessment by means of optical flow analysis of phase-contrast microscopy images. Computerized Medical Imaging and Graphics, 2014, 38, 163-170.	5.8	8
83	Automatic left ventricle volume calculation with explainability through a deep learning weak-supervision methodology. Computer Methods and Programs in Biomedicine, 2021, 208, 106275.	4.7	8
84	Brain Network Allostasis after Chronic Alcohol Drinking Is Characterized by Functional Dedifferentiation and Narrowing. Journal of Neuroscience, 2022, 42, 4401-4413.	3.6	8
85	Routing Design in Wireless Sensor Networks and a Solution for Healthcare Environments. IEEE Latin America Transactions, 2011, 9, 408-414.	1.6	7
86	Head-to-head comparison of 1 week versus 6 months CMR-derived infarct size for prediction of late events after STEMI. International Journal of Cardiovascular Imaging, 2013, 29, 1499-1509.	1.5	7
87	Open Source 3D Printed Lung Tumor Movement Simulator for Radiotherapy Quality Assurance. Materials, 2018, 11, 1317.	2.9	7
88	A Novel Clinical and Stress Cardiac Magnetic Resonance (C-CMR-10) Score to Predict Long-Term All-Cause Mortality in Patients with Known or Suspected Chronic Coronary Syndrome. Journal of Clinical Medicine, 2020, 9, 1957.	2.4	7
89	Risk score for early risk prediction by cardiac magnetic resonance after acute myocardial infarction. International Journal of Cardiology, 2022, 349, 150-154.	1.7	7
90	Tractography of the uncinate fasciculus and the posterior cingulate fasciculus in patients with mild cognitive impairment and Alzheimer disease. NeurologÃa (English Edition), 2014, 29, 11-20.	0.4	6

#	Article	IF	CITATIONS
91	Automatic segmentation of the spine by means of a probabilistic atlas with a special focus on ribs suppression. Medical Physics, 2017, 44, 4695-4707.	3.0	6
92	Volume Mesh Generation and Finite Element Analysis of Trabecular Bone Magnetic Resonance Images. Annual International Conference of the IEEE Engineering in Medicine and Biology Society, 2007, 2007, 1603-6.	0.5	5
93	Functional diffusion map: A biomarker of brain metastases response to treatment based on magnetic resonance image analysis. , 2015, 2015, 4282-5.		5
94	HIVE Tracker. , 2018, , .		5
95	A generalized entropy-based two-phase threshold algorithm for noisy medical image edge detection. Scientia Iranica, 2017, .	0.4	5
96	Shortâ€Term Changes in Left and Right Ventricular Cardiac Magnetic Resonance Feature Tracking Strain Following Ferric Carboxymaltose in Patients With Heart Failure: A Substudy of the Myocardialâ€IRON Trial. Journal of the American Heart Association, 2022, 11, e022214.	3.7	5
97	Quantitative analysis of cerebrospinal fluid flow in complex regions by using phase contrast magnetic resonance imaging. International Journal of Imaging Systems and Technology, 2011, 21, 290-297.	4.1	4
98	Optical flow method in phase-contrast microscopy images for the diagnosis of primary ciliary dyskinesia through measurement of ciliary beat frequency. Preliminary results. , 2012, , .		4
99	Brain size regulations by cbp haploinsufficiency evaluated by in-vivo MRI based volumetry. Scientific Reports, 2015, 5, 16256.	3.3	4
100	Automatic segmentation of the spine by means of a probabilistic atlas with a special focus on ribs suppression. Preliminary results. , 2015, 2015, 2014-7.		4
101	Brain functional connectivity alterations in a rat model of excessive alcohol drinking: A resting-state network analysis. , 2017, 2017, 3016-3019.		4
102	A Tangible Educative 3D Printed Atlas of the Rat Brain. Materials, 2018, 11, 1531.	2.9	4
103	ALTEA: A Software Tool for the Evaluation of New Biomarkers for Alzheimer's Disease by Means of Textures Analysis on Magnetic Resonance Images. Diagnostics, 2018, 8, 47.	2.6	4
104	Longitudinal strain in remote non-infarcted myocardium by tissue tracking CMR: characterization, dynamics, structural and prognostic implications. International Journal of Cardiovascular Imaging, 2021, 37, 241-253.	1.5	4
105	A semiautomatic segmentation method, solid tissue classification and 3D reconstruction of mandible from computed tomography imaging for biomechanical analysis. , 2012, , .		3
106	A fully automated method for spinal canal detection in computed tomography images. , 2014, 2014, 5514-7.		3
107	Identifying the primary site of origin of MRI brain metastases from lung and breast cancer following a 2D radiomics approach. , 2017, , .		3
108	Texture analysis for infarcted myocardium detection on delayed enhancement MRI. , 2017, , .		3

Texture analysis for infarcted myocardium detection on delayed enhancement MRI. , 2017, , . 108

#	Article	IF	CITATIONS
109	Combined assessment of stress cardiovascular magnetic resonance and angiography to predict the effect of revascularization in chronic coronary syndrome patients. European Journal of Preventive Cardiology, 2022, 29, 407-416.	1.8	3
110	Performance Study of Convolutive BSS Algorithms Applied to the Electrocardiogram of Atrial Fibrillation. Lecture Notes in Computer Science, 2006, , 495-502.	1.3	3
111	Neuroimaging reveals functionally distinct neuronal networks associated with high-level alcohol consumption in two genetic rat models. Behavioural Pharmacology, 2021, 32, 229-238.	1.7	3
112	Myocardial Echocardiography With Intracoronary Injection of Contrast in Post-Infarction Patients. Implications and Comparison With Angiography and Magnetic Resonance Imaging. Revista Espanola De Cardiologia (English Ed ), 2004, 57, 20-28.	0.6	2
113	Additional Diagnostic Value of Systolic Dysfunction Induced by Dipyridamole Stress Cardiac Magnetic Resonance Used in Detecting Coronary Artery Disease. Revista Espanola De Cardiologia (English Ed ), 2009, 62, 383-391.	0.6	2
114	Magnetic resonance imaging gridding reconstruction methods with and without density compensation functions. IEEE Latin America Transactions, 2011, 9, 774-778.	1.6	2
115	Principles of Computational Modelling in Neuroscience [Book Reviews]. IEEE Pulse, 2012, 3, 82-82.	0.3	2
116	Ciliary motility activity measurement using a dense optical flow algorithm. , 2013, 2013, 4446-9.		2
117	Fully automatic spinal canal segmentation for radiation therapy using a Gradient Vector Flow-based method on computed tomography images: A preliminary study. , 2014, 2014, 5518-21.		2
118	Evaluating network brain connectivity in alcohol postdependent state using Network-Based Statistic. , 2017, 2017, 533-536.		2
119	Functional MRI of Synaptic Plasticity. Handbook of Behavioral Neuroscience, 2018, 28, 441-456.	0.7	2
120	Medical Mechatronics for Healthcare. Journal of Healthcare Engineering, 2018, 2018, 1-3.	1.9	2
121	Determination of Non-Invasive Biomarkers for the Assessment of Fibrosis, Steatosis and Hepatic Iron Overload by MR Image Analysis. A Pilot Study. Diagnostics, 2021, 11, 1178.	2.6	2
122	Determination of Image-based Biomarkers for the Diagnosis of Hypertrophic Cardiomyopathy, Hypertensive Cardiomyopathy and Amyloidosis From Texture Analysis in Cardiac MRI. , 2020, , .		2
123	PSPU-Net for Automatic Short Axis Cine MRI Segmentation of Left and Right Ventricles. , 2020, , .		2
124	Low-Power Lossless Data Compression for Wireless Brain Electrophysiology. Sensors, 2022, 22, 3676.	3.8	2
125	Epicardial atrial activation assessment from the surface ECG in atrial fibrillation. , 2005, , .		1

Atrial activity enhancement by blind sparse sequential separation. , 2005, , .

1

#	Article	IF	CITATIONS
127	ICARO: a computer aided diagnosis tool for the quantification of intracoronary and intravenous echocardiography. , 2005, , .		1
128	Sharing acute myocardial infarction databases through the internet with MySQL and PHP: A web-accessible database for clinical research networks. , 2007, , .		1
129	Ventricular Artifacts Cancellation from Atrial Epicardial Recordings in Atrial Tachyarrhythmias. Annual International Conference of the IEEE Engineering in Medicine and Biology Society, 2007, 2007, 6504-7.	0.5	1
130	Estimating intracranial fluid dynamics using quantitative analyses of phase contrast magnetic resonance images. Radiologia, 2010, 52, 51-57.	0.5	1
131	Medical Imaging: Principles, Detectors, and Electronics (Iniewski, K., Ed.; 2009) [Book Reviews]. IEEE Pulse, 2011, 2, 76-77.	0.3	1
132	Automatic detection of local arterial input functions through Independent Component Analysis on Dynamic Contrast enhanced Magnetic Resonance Imaging. , 2015, 2015, 4294-7.		1
133	Magnetic resonance microimaging of a swine infarcted heart: Performing cardiac virtual histologies. , 2015, 2015, 1584-7.		1
134	Automatic Brain Morphometry and Volumetry Using SPM on Cognitively Impaired Patients. IEEE Latin America Transactions, 2015, 13, 1077-1082.	1.6	1
135	Comment on "Computer-Extracted Texture Features to Distinguish Cerebral Radionecrosis from Recurrent Brain Tumors on Multiparametric MRI: A Feasibility Studyâ€: American Journal of Neuroradiology, 2017, 38, E21-E21.	2.4	1
136	RATT: RFID Assisted Tracking Tile. Preliminary results. , 2017, 2017, 4114-4117.		1
137	TherMouseDuino: An affordable Open-Source temperature control system for functional magnetic resonance imaging experimentation with mice. Magnetic Resonance Imaging, 2019, 58, 67-75.	1.8	1
138	A Ciliary Motility Index for Activity Measurement in Cell Cultures With Respiratory Syncytial Virus. American Journal of Rhinology and Allergy, 2019, 33, 121-128.	2.0	1
139	Derivation of Atrial Surface Reentries Applying ICA to the Standard Electrocardiogram of Patients in Postoperative Atrial Fibrillation. Lecture Notes in Computer Science, 2006, , 478-485.	1.3	1
140	Microfinite Element Modeling for Evaluating Polymer Scaffolds Architecture and their Mechanical Properties from microComputed Tomography. , 0, , .		1
141	Finite Element Modeling for a Morphometric and Mechanical Characterization of Trabecular Bone from High Resolution Magnetic Resonance Imaging. , 0, , .		1
142	Predictive Value of Cardiac Magnetic Resonance Feature Tracking after Acute Myocardial Infarction: A Comparison with Dobutamine Stress Echocardiography. Journal of Clinical Medicine, 2021, 10, 5261.	2.4	1
143	End-systole and end-diastole detection in short axis cine MRI using a fully convolutional neural network with dilated convolutions. Computerized Medical Imaging and Graphics, 2022, 99, 102085.	5.8	1
144	SAGIMA: an easy-to-use and low cost WEB-PACS system for an optimal access and management of a digital angiography database. , 2005, , .		0

#	Article	IF	CITATIONS
145	Feasibility and performance of methods based on statistical signal processing to study atrial fibrillation. , 2005, , .		0
146	Clinical Software for the Assessment of Trabecular Bone Disease in Distal Radius Based on a Magnetic Resonance Structural Analysis. Annual International Conference of the IEEE Engineering in Medicine and Biology Society, 2007, 2007, 2073-6.	0.5	0
147	Comparison of atrial wave extraction methods from invasive recordings in atrial fibrillation. , 2007, ,		0
148	ICA for Ovary Tissue Classification of Perfusion Magnetic Resonance Images. Annual International Conference of the IEEE Engineering in Medicine and Biology Society, 2007, 2007, 1611-4.	0.5	0
149	Time-resolved parallel imaging with a reduced dynamic field of view. , 2008, , .		0
150	Microscopic Image Analysis for Life Science Applications (Rittscher, J. et al., Eds.; 2008) [Book Reviews. IEEE Engineering in Medicine and Biology Magazine, 2010, 29, 106-107.	0.8	0
151	Morphological and statistical analysis of biomaterials with applications in tissue engineering by means of microscopy image processing. IEEE Latin America Transactions, 2011, 9, 399-407.	1.6	0
152	Comparison of the main magnetic resonance imaging acceleration strategies based on parallel imaging techniques. IEEE Latin America Transactions, 2011, 9, 749-758.	1.6	0
153	Signal Analysis Techniques (Blinowska, K.J. and Zygierewicz, J.; 2012) [Book Review]. IEEE Pulse, 2012, 3, 60-60.	0.3	0
154	Optimal sampling for "Noquist―reduced-data cine magnetic resonance imaging. Medical Physics, 2012, 40, 012302.	3.0	0
155	P-53RESTING-STATE BRAIN NETWORKS DURING HIGH LEVELS OF ALCOHOL DRINKING FOLLOWED BY ABSTINENCE IN RATS. Alcohol and Alcoholism, 2015, 50, i58.4-i59.	1.6	0
156	SY27-3LONGITUDINAL STUDY OF FUNCTIONAL AND MICROSTRUCTURAL ALTERATIONS IN BRAIN NETWORKS DURING ALCOHOL INTOXICATION AND ABSTINENCE. Alcohol and Alcoholism, 2015, 50, i30.3-i30.	1.6	0
157	PETra: software tool for a semiautomatic positron emission tomography image analysis and its application to the study of brain glucose consumption in rats. IEEE Latin America Transactions, 2015, 13, 876-884.	1.6	0
158	Development of functional and structural brain alterations in logitudinal models of high alcohol consumption and abstinence. Alcohol, 2017, 60, 215.	1.7	0
159	A fully automated method for segmentation and classification of local field potential recordings. Preliminary results. , 2017, 2017, 426-429.		0
160	Automatic positioning device for cutting three-dimensional tissue in living or fixed samples. Proof of concept. , 2017, 2017, 1372-1375.		0
161	The use of subject-specific Finite Element analysis of L1-L4 vertebra to screening osteoporosis in postmenopausal women. , 2017, 2017, 1832-1835.		0
162	OncoSpineSeg: A Software Tool for a Manual Segmentation of Computed Tomography of the Spine on Cancer Patients. , 2017, , .		0

#	Article	IF	CITATIONS
163	EP-2080: Dual-energy computed tomography and prediction of response to radiotherapy treatment in lung cancer. Radiotherapy and Oncology, 2018, 127, S1141-S1142.	0.6	Ο
164	Sequential cardiovascular magnetic resonance assessment of left ventricular ejection fraction for prediction of subsequent events in a large multicenter STEMI registry. European Heart Journal Cardiovascular Imaging, 2021, 22, .	1.2	0
165	Dual Energy Computed Tomography for Lung Cancer Diagnosis and Characterization. , 2019, , 49-74.		0
166	DEVELOPING EXPERIMENTAL DESIGN AND ANALYTICAL SKILLS IN METABOLOMICS: A BIOMEDICAL ENGINEERING LABORATORY EXPERIMENT PROPOSAL. , 2020, , .		0
167	Comparative Analysis of Tagging and Feature-Tracking Cardiac MRI Techniques for the Evaluation of Cardiac Deformation. , 2020, , .		Ο
168	Sex Effect in the Decision to Perform Invasive Coronary Angiography in Patients With Chronic Coronary Syndrome After Undergoing Vasodilator Stress <scp>MRI</scp> . Journal of Magnetic Resonance Imaging, 2022, , .	3.4	0